



HAL
open science

Statics and Dynamics of Adhesion between Two Soap Bubbles

Sébastien Besson, Georges Debrégeas

► **To cite this version:**

Sébastien Besson, Georges Debrégeas. Statics and Dynamics of Adhesion between Two Soap Bubbles. 2007. hal-00136883v3

HAL Id: hal-00136883

<https://hal.science/hal-00136883v3>

Preprint submitted on 19 Mar 2007 (v3), last revised 16 Aug 2007 (v4)

HAL is a multi-disciplinary open access archive for the deposit and dissemination of scientific research documents, whether they are published or not. The documents may come from teaching and research institutions in France or abroad, or from public or private research centers.

L'archive ouverte pluridisciplinaire **HAL**, est destinée au dépôt et à la diffusion de documents scientifiques de niveau recherche, publiés ou non, émanant des établissements d'enseignement et de recherche français ou étrangers, des laboratoires publics ou privés.

Statics and dynamics of adhesion between two soap bubbles

S. Besson, G. Debrégeas

Laboratoire de Physique Statistique, CNRS UMR 8550,
24, rue Lhomond, 75231 Paris Cedex 05, France

19th March 2007

Abstract An original set-up is used to study the adhesive properties of two hemispherical soap bubbles put into contact. The contact angle at the line connecting the three films is extracted by image analysis of the bubbles profiles. After the initial contact, the angle rapidly reaches a static value slightly larger than the standard 120° angle expected from Plateau rule. This deviation is consistent with previous experimental and theoretical studies: it can be quantitatively predicted by taking into account the finite size of the Plateau border (the liquid volume trapped at the vertex) in the free energy minimization. The visco-elastic adhesion properties of the bubbles are further explored by measuring the deviation $\Delta\theta_d(t)$ of the contact angle to the static value, as the distance between the two bubbles is sinusoidally modulated. It is found to linearly increase with the imposed displacement amplitude. The in-phase and out-of-phase components of $\Delta\theta_d(t)$ with the imposed modulation frequency are systematically probed, which reveals a transition from a viscous to an elastic response of the system with a crossover frequency of the order 0.2Hz. Independent interfacial rheological measurements, obtained from an oscillating bubble experiment, allow us to test several modes of deformation of the surfactant monolayers. The relevance of such adhesive dynamic properties to the rheology of foams is briefly discussed using a perturbative approach to Princen 2D model of foams.

PACS. 47.55.D- Drops and bubbles – 47.55.dk Surfactant effects – 83.80.Iz Emulsions and foams

1 Introduction

Liquid foams are concentrated dispersions of gas bubbles in a liquid matrix. Their mechanical properties have been the focus of a number of studies in the recent past [1,2,3]. Liquid foams exhibit quasi-elastic behavior up to a finite yield stress or strain beyond which they flow like shear-thinning viscous liquids. Most of the elastic response originates from the variation of the total film area induced by an applied shear. The resulting shear modulus scales as $\mu = 2\gamma/R$ where 2γ is the surface tension of the soap film, and R the average radius of the bubbles. The dissipation is controlled, in major part, by irreversible rearrangements of the bubbles (T1 events).

Other mechanisms of energy storage and dissipation however contribute to the viscoelastic moduli of the foam. They have been thoroughly discussed theoretically by Buzza and Schwartz [4,5]. One is associated with the interfacial viscoelasticity of the soap films, which can be independently measured using a wide range of experimental techniques (oscillating barriers [6,7], thin-film interfaces [8], oscillating bubble/drop [9,10]). They all consist in submitting a single mono- or bi-layer to an oscillating stretching while measuring the evolution of the surface tension. The second source of dissipation takes place in the Plateau borders, the region of the foam where the films meet and where most of the liquid content is trapped. As the foam is strained, the Plateau borders move relatively to the soap films to which they are connected, inducing dissipative viscous flows. This viscous drag force has been extensively studied but

only in a situation where the Plateau border is in contact with a solid surface [11,12,13,14].

Relating these local measurements (interfacial rheology and Plateau border viscous drag force) to the global rheology of the foams is tricky. First, it is difficult to actually separate the different modes of dissipation. In a real foam, Ostwald ripening (the disproportionation of bubbles induced by gas diffusion through the films) induce T1 events even in the absence of an imposed strain. Second, due to the many modes of accessible deformation, the motion of the vertices in a foam under simple strain is not affine. Describing their trajectory becomes extremely difficult when the foam is polydisperse.

Beyond these issues, one can also question the relevance of measurements performed with an isolated film to describe the behavior of a macroscopic foam. In all the techniques currently used to estimate the rheological properties of the films, the surfactant layers are confined by solid barriers. In contrast, films in a real foam are bounded by fluid Plateau borders which may allow the transfer of surfactants from one side to another. In the case of Plateau border viscous drag, the situation is even worst: the resistance to motion is measured by dragging a Plateau border along a solid wall, which imposes a very different hydrodynamic boundary to the flow as compared to a self supported Plateau border.

One attempt to extract information about local dissipation within a macroscopic foam has been recently proposed by Durand and Stone [15]. They optically studied the dynamic of T1 events in a confined 2D foam (a monolayer of bubbles squeezed

between two solid plates) and were able to relate the duration of the plastic process with intrinsic rheological properties of the soap films. This experiment has two limitations: first, the friction of the Plateau borders on the confining walls induce viscous dissipation. Second, the use of T1 events as the deformation mechanism does not allow one to modulate in a controlled way the dynamics of local deformation of the set of bubbles (although this might actually be feasible with minor modification of the authors' experimental procedure).

In this article, we propose a new approach to study local elastic and dissipative processes in a configuration more directly amenable to 3D foams. Two hemispherical bubbles are put into contact and their relative distance is modulated at various frequencies. In this configuration, the central film separating the two bubbles is bounded by a self-supported Plateau border whose radius oscillates with the distance between the two bubbles. We focus on angular measurements at the contact line which provides most of the relevant information concerning the elastic and dissipation processes.

The article is organized as follows. In part 2, the experimental set-up, the optical measurements and image analysis are detailed. The static results of contact angle measurements are presented in part 3, together with data obtained from a numerical simulation. Part 4 focuses on dynamic properties of adhesion and also presents the results of standard rheological interfacial measurements performed on single films using the same soap solution. These results are discussed in part 5: two different models of monolayers stretching are discussed and their predictions are confronted to the angular measurements. In part 6, the application of these angular measurements to the rheology of foams is discussed within the scope of Princen 2D hexagonal model [16]. Conclusion and perspectives are drawn in part 7.

2 Experiments

An hemispherical bubble is formed by blowing air at the cone-shaped end of a stainless steel tube, of external radius $R = 7\text{mm}$, filled with a soap solution (figure 1). The liquid in the tube is connected through a porous disk (Duran, diameter 2.8mm , height 5mm) to a reservoir. Once the bubble is formed, the reservoir is lowered a few centimeters to impose a small negative pressure difference between the liquid and gas phases. The disk porosity is fine enough (poresize $10\text{-}16\ \mu\text{m}$) to prevent the bubble from being sucked down. The entire device is enclosed in a glass cell ($40 \times 40 \times 40\text{cm}$) to limit evaporation and increase the bubbles lifetime. In all the experiments, the soap solution is made of tetramethyltetradecylammonium bromide (TTAB purchased from Sigma-Aldrich) 3g/L in a water/glycerol mixture (volume ratio of $75/25$).

This device is used in two types of experiments. In single bubble experiments, a section of the air tube is squeezed between two parallel plates whose separation can be sinusoidally modulated using a DC motor (Newport, LTA-HS). A pressure sensor (Validyne, DP103) allows us to simultaneously monitor the pressure drop between the inside and outside of the bubble. In the double bubble setup, a similar device is placed on top of the first one (figure 1) and their axis are carefully aligned using

two cameras. The top device is mounted on a vertical displacement stage attached to the DC motor.

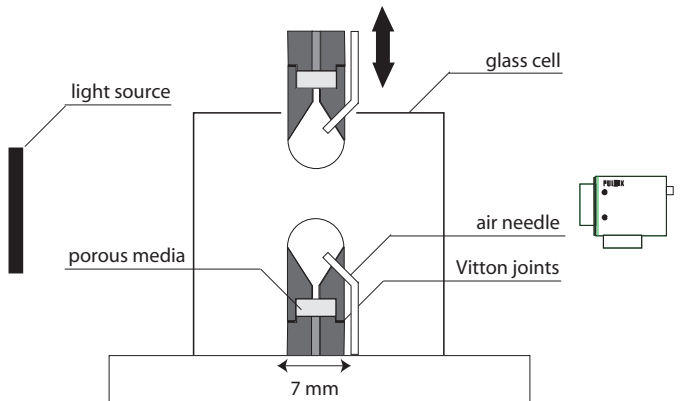


Figure 1. Schematic of the experimental double bubble device.

The set-up is illuminated by a diffusive light source (Schott, Backlight). The shadow image of the bubbles is captured on a CCD-camera equipped with a telecentric objective (Navitar, 6X) to allow accurate angular and length measurements. Depending on the studied frequency, two cameras are used: a Pulnix TM-1320 CL and a Mikrotron MC1310 with frame rates up to 15 frames/s and 240 frames/s respectively. Image capture is synchronized with the motor motion and pressure recording. The bubbles profiles are extracted by image analysis with a sub-pixel resolution using the software IDL (see figure 2(c)). The symmetry axis is determined and defines the cylindrical coordinates (r, z) . For both bubbles, the profiles $r(z)$ are fitted to the Laplace equation which relates the local curvature $\frac{1}{R'} + \frac{1}{R''}$ to the pressure drop ΔP across the film:

$$\Delta P = 2\gamma \left(\frac{1}{R'} + \frac{1}{R''} \right) \quad (1)$$

$$\frac{r(z)}{\sqrt{1+r'(z)^2}} = \frac{\Delta P}{4\gamma} r(z)^2 + \lambda \quad (2)$$

where 2γ is the surface tension of the soap film; the parameter λ results from the integration of equation (1) and is set by the boundary conditions. For each bubble, the set of parameters $\left(\frac{\Delta P}{4\gamma}, \lambda \right)$ is extracted from the best fit of the region of the profiles outside the Plateau borders. The prolongations of the reconstructed profiles intersect in the Plateau border and define a contact radius r_c and a contact angle θ as shown in figure 2(c). Similarly, the three interfaces which delimit the Plateau border obey the same equation (2) with the term $\frac{\Delta P}{4\gamma}$ replaced by $\frac{\Delta P}{2\gamma}$ since these are single air/water interfaces. Here ΔP corresponds to the pressure difference between the liquid in the Plateau border and the gas phase (bubble or atmosphere). By fitting the external profile, we extract the set of parameters $\left(\frac{\Delta P}{2\gamma}, \lambda_l \right)$ and reconstruct the Plateau border (see figure 2(d)).

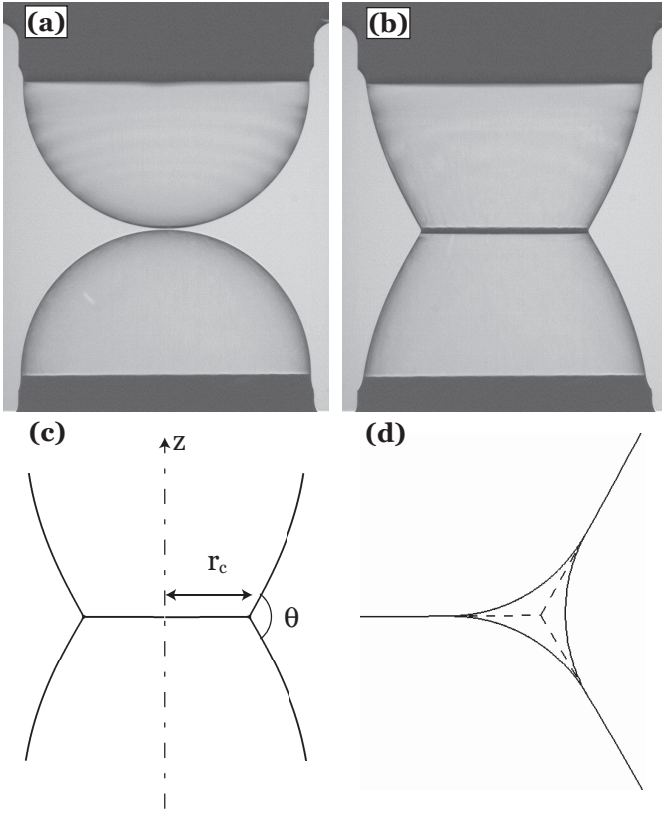


Figure 2. Images of a double bubble static adhesion experiment (a) before contact and (b) just after contact. Results of the image analysis: (c) external profiles fitted by the Laplace equation from which the central film radius r_c and contact angle θ are extracted, (d) reconstructed Plateau border.

3 Static correction to Plateau rule

In this part, we report on static measurements of the contact angle θ . Two bubbles are brought into contact at vanishing low speed. Time 0 is defined by the image of the first contact. The time evolution of the central film radius r_c and contact angle θ at short times are shown on figure 3. It exhibits a transient of a few seconds during which both parameters significantly vary. The first $\sim 0.1s$ corresponds to the rapid formation of the central film: only the end of this phase can be captured even with the fast camera. During the next few seconds, the radius and contact angle keep increasing. This second stage is associated with the capillary drainage of the freshly formed film toward the Plateau border which allows pressure equilibration within the liquid phase. This process can be monitored by measuring the evolution of the Plateau border height (see figure 3). For $t \gtrsim 10s$, the system is equilibrated (figure 4) but a slow decay of r_c is still observable due to gas diffusion through the films. This process does not affect the value of the contact angle θ which remains constant until the bubbles breakup (after a few minutes).

We define θ_{eq} as the value of the contact angle for time $t > 10s$. For all experiments, θ_{eq} is found to be larger than 120° as predicted by Plateau rule [17]. Such a deviation has been previously observed in various experiments [18, 19, 20]. In the last reference, similar measurements were performed on

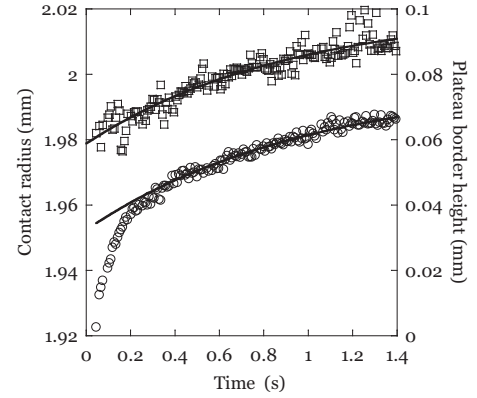


Figure 3. Short-times evolution of the contact radius (circles) and the Plateau border height (squares) as a function of time for two contacting bubbles. During the first 0.2s, the fast rise of the contact radius corresponds to the initial growth of the central film. After 0.2s, the evolution of the contact radius is to be compared to the one of the Plateau border height. Both series of measurements are adjusted by rising exponential fits of the type $x_0 + \Delta x e^{-\frac{t}{\tau}}$ (solid lines) and highlight a characteristic time τ of the order of 1s.

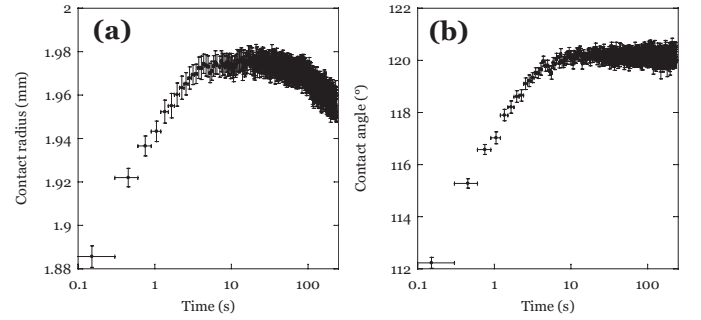


Figure 4. Long-times evolution of (a) the contact angle and (b) the contact radius as a function of the time during a contacting bubbles experiment. After an initial growth, both series reach constant values, the contact angle value being slightly higher than the predicted 120° from the Plateau rule. The decay of the contact radius after 60s is attributed to the gas diffusion outside the bubble. The experiment ends up when one of the two bubbles break.

a single catenoid separated by a soap film. The contact angle between both catenoidal films was found to grow linearly with the ratio $\frac{r_{PB}}{r_c}$ where r_{PB} is the Plateau border curvature radius and r_c the central film radius.

This deviation can be qualitatively understood by first considering an infinitely dry foam. In this case, the force equilibrium at the contact line imposes the three films to meet at 120° . Decorating the line with a Plateau border reduces the total area of the films by a quantity $2S_{dry} - S_{PB}$ [21] which is a (negative) decreasing function of the Plateau border volume. The presence of a Plateau border is thus associated with a negative line tension. In the specific case of the double bubble, this effect has been described by Fortes and Teixeira [22]. They predict a contact angle in the presence of Plateau border given by:

$$\theta_{eq} = 120 + \frac{180}{\pi} \frac{1}{4\pi r_c^2 \sqrt{3}} (2S_{dry} - S_{PB}) \quad (3)$$

In order to test this expression, several contacting bubbles experiments are performed with different values of contact radius and Plateau border size. For each of them, the final value of the contact angle as well as $S_{dry} - S_{PB}$ are measured. Figure 5 shows the measured angle θ_{eq} as a function of the predicted result obtained from equation (3).

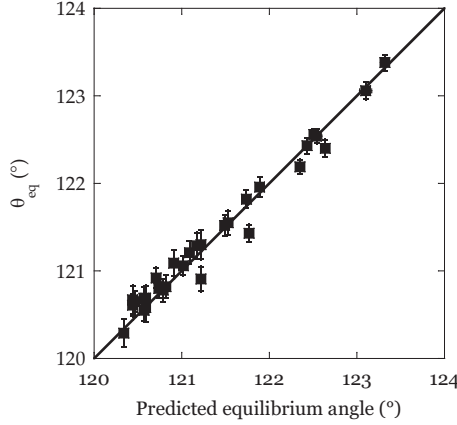


Figure 5. Experimental static contact angle θ_{eq} as a function of the angle predicted by Fortes law (equation 3) for various values of the radius r_c and the Plateau border volume.

This result was independently confirmed by simulations of the double bubble experiment carried out using Surface Evolver [23]. This software allows one to calculate minimal surface configurations under a given set of conditions. Two contacting bubbles of fixed volume are generated with different volumes of the Plateau border. After several minimization cycles, the equilibrated configuration is treated the same way as for the experiments. Figure 6 shows the numerical contact angle versus the predicted contact angle value for various Plateau border volumes.

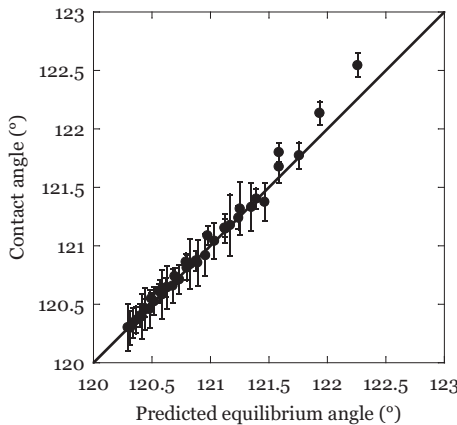


Figure 6. Numerical contact angle obtained from Surface Evolver simulations as a function of the angle predicted by Fortes law (equation 3) for various values of the imposed Plateau border volume.

The agreement of the experimental and numerical results with Fortes and Teixeira's model validates the decoration law

for the double bubble. It also demonstrates the accuracy of the angle measurement procedure. In the rest of the article, expression 3 will be used in order to calculate, at any moment, the equilibrium contact angle $\theta_{eq}(t)$. This reference angle will be subtracted from the measured angle in order to extract the dynamic deviation $\Delta\theta_d = \theta(t) - \theta_{eq}(t)$.

4 Dynamics of adhesion

In order to probe the dynamic response of the contact angle, a sinusoidal displacement of the upper tube is applied at controlled frequencies in the range 0.01-20 Hz. The double bubble is prepared as previously described. Successive contacts and separations of the bubbles allow one to progressively reduce the volume of liquid trapped in the Plateau border. All experiments are performed with a contact radius $r_c \approx 2\text{mm}$ and a Plateau border height $h_{PB} \approx 0.2\text{mm} \ll r_c$. Figure 7 shows the typical time evolution of $r_c(t)$ and $\theta(t)$. The corrected contact angle, $\theta_{eq}(t)$ calculated from equation 3, varies between 120.50° and 120.56° . Therefore, the main contribution to the observed oscillation of $\theta(t)$ is due to dynamic effects. The evolution of these two parameters are decomposed as:

$$r_c(t) = r_c^0 + \Delta r_c(\omega) \cos(\omega t) \quad (4)$$

$$\Delta\theta_d(t) = \Delta\theta(\omega) \cos(\omega t + \phi(\omega)) \quad (5)$$

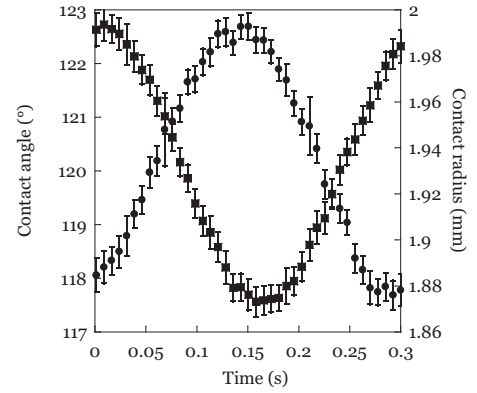


Figure 7. Evolution of the contact radius (squares) and the contact angle (circles) as a function of the time over an oscillating period for an oscillating amplitude of 0.2mm at a frequency of 3Hz. The error bars are calculated from the uncertainties on the fitting parameters (equation 2). Typical standard deviations are equal to $7\mu\text{m}$ for the contact radius and 0.2° for the contact angle.

It should be noted that r_c^0 is not strictly constant : it slightly decreases as a consequence of the gas diffusion (figure 4(b)). To precisely measure $r_c(\omega)$, $\Delta\theta(\omega)$ and $\phi(\omega)$, $r_c(t)$ and $\Delta\theta_d(t)$ are therefore filtered to extract the Fourier component associated with the imposed frequency. Figure 8 shows the dependence of $\Delta\theta$ with $\Delta r_c/r_c^0$ for three different oscillation frequencies. It shows that the contact angle response is linear with the imposed solicitation. This allows one to define two moduli associated with the in-phase and out-of-phase responses of the contact angle to the modulation of the contact radius:

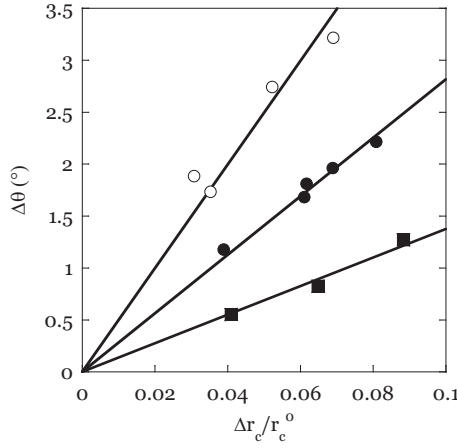


Figure 8. Linearity of the amplitude of the dynamic angle deviation with the amplitude of the normalized contact radius variations at different frequencies. Squares: 0.2Hz. Circles: 1Hz. Diamonds: 5Hz.

$$G'(\omega) = -\frac{\Delta\theta(\omega)}{\Delta r_c(\omega)} r_c^0 \cos(\phi(\omega)) \quad (6)$$

$$G''(\omega) = \frac{\Delta\theta(\omega)}{\Delta r_c(\omega)} r_c^0 \sin(\phi(\omega)) \quad (7)$$

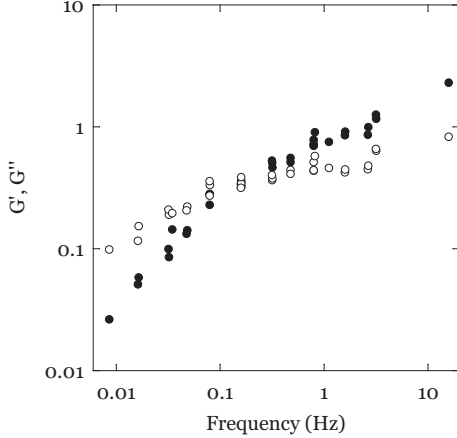


Figure 9. Evolution of the angular elastic and viscous moduli, estimated from equation (6) and (7), with the frequency of the oscillation. Closed circles: elastic modulus. Open circles: loss modulus.

Figure 9 shows the evolution of G' and G'' as the frequency is varied over 3 decades. It reveals a transition from a viscous regime at low frequency to an elastic regime at high frequency, with a crossover around 0.2Hz.

The existence of an in-phase component of the dynamic angle signal cannot be accounted for by dissipation in the Plateau border alone. In contrast, it can be understood by considering the viscoelastic behavior of the soap films [24, 15]. As the distance between the bubbles are modulated, the films area varies which in turn induces a variation of their surface tension. In Gibbs approach, the surface tension $\gamma(t)$ associated with a si-

nusoidal modulation of the film surface area $S(t) = S^0 + \Delta S \cos(\omega t)$ is written, in the limit $\Delta S/S^0 \approx 0$:

$$\gamma(t) = \gamma_0 + E'(\omega) \frac{\Delta S}{S^0} \cos(\omega t) + E''(\omega) \frac{\Delta S}{S^0} \sin(\omega t) \quad (8)$$

where $\tilde{E}(\omega) = E'(\omega) + iE''(\omega)$ is the Gibbs complex modulus [25, 26]. This parameter can be independently evaluated by sinusoidally modulating the volume of a single bubble while recording its radius R and the internal pressure P , from which its surface tension $2\gamma = P/2R$ and area can be calculated. The frequency diagram of both moduli are plotted on figure 10.

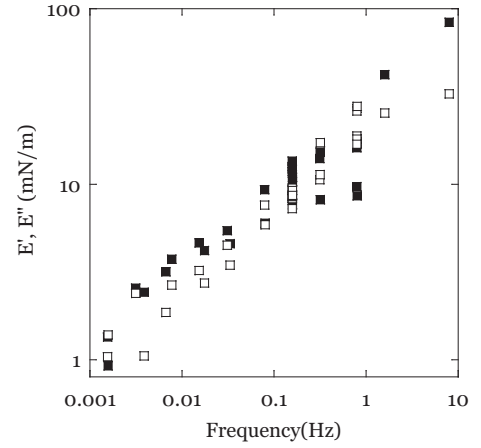


Figure 10. Evolution of the Gibbs elastic and viscous moduli with the frequency of the oscillation for an oscillating bubble experiment. Closed squares: elastic modulus. Open squares: viscous modulus. The dispersion is mainly due to uncertainties on the measurement of the internal pressure.

5 Interpretation

In this section, we attempt to relate the double-bubble angular measurements to the film rheological moduli obtained from the single oscillating bubble experiment. This requires to describe the evolution of each monolayer that form the double bubble system. Two situations are successively examined which should correspond to small and large values of the ratio $\mu_s/\mu_l h$, where μ_s is the film viscosity, μ_l is the solution bulk viscosity and h is the thickness of the films.

5.1 Adhesive monolayers

When $\mu_s \ll \mu_l h$, surfactant monolayers are adhesive: the viscosity of the intercalated fluid layer inhibit any relative motion between them. In this situation, one needs to consider separately the central film, characterized at each time by its area and surface tension ($S_1, 2\gamma_1$), and the two outer films similarly characterized by ($S_2, 2\gamma_2$)¹. Within this hypothesis, the evolution of γ_i and S_i are related through equation 8. Measurements

¹ the system is assumed to be symmetric, which is the case in all experiments, so that the outer film have identical characteristics

of the different surface areas in both the experiments and the Surface Evolver simulations show that $S_1(t) + S_2(t)$ is a constant equal to $2\pi R^2$ for initially hemispherical bubbles. The variations ΔS_i and Δr_c (with respect to their equilibrated values S_i and r_c) are thus simply related, to first order, through:

$$\frac{\Delta S_1}{S_1^0} = \frac{2\Delta r_c}{r_c^0} \quad (9)$$

$$\frac{\Delta S_2}{S_2^0} = \frac{2r_c^0 \Delta r_c}{2R^2 - r_c^{02}} \quad (10)$$

As the distance between bubbles is modulated, the three films experience cycles of compression and stretching which in turn modulate their surface tensions $2\gamma_1$ and $2\gamma_2$ (figure 11(a)). Defining $2\Delta\gamma_1$ and $2\Delta\gamma_2$ as the instantaneous deviations to the equilibrium surface tension $2\gamma_0$, force equilibrium at the intersection point between the three interfaces yields (in the limit $\Delta\theta_d \ll 1$):

$$\frac{\sqrt{3}}{2}\gamma_0\Delta\theta_d(t) = \Delta\gamma_1(t) - \Delta\gamma_2(t) \quad (11)$$

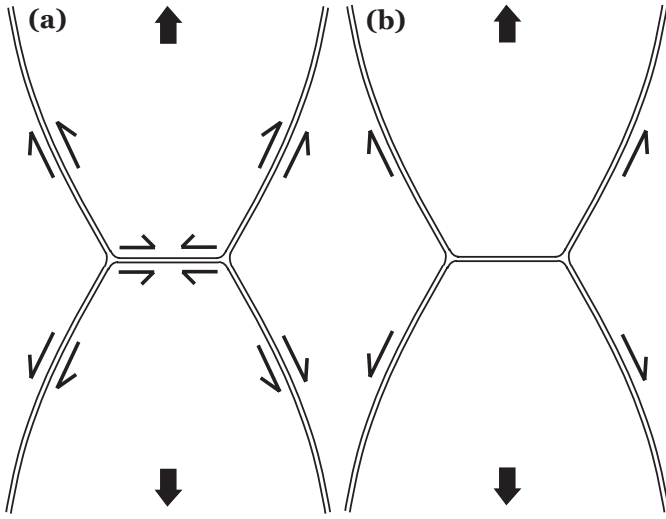


Figure 11. Models of compression/stretching of the monolayers for a double bubble submitted to an oscillating sollicitation. (a) When $\mu_s \ll \mu_l h$, the monolayers are adhesive and the three films are stretched independently. (b) When $\mu_l h \ll \mu_s$, the monolayers are able to slide over one another. Only the outer monolayer is actually stretched since the internal monolayer area remains constant to the first order.

By combining equations (6), (7), (8), (10), and (11), one can predict, within these hypothesis, the expression of G' and G'' as a function of the Gibbs moduli as:

$$\gamma_0 G' = f(r_c^0, R) E' \quad (12)$$

$$\gamma_0 G'' = f(r_c^0, R) E'' \quad (13)$$

with

$$f(r_c^0, R) = \frac{2}{\sqrt{3}} \frac{4R^2}{(2R^2 - r_c^{02})} \quad (14)$$

5.2 Sliding monolayers

A different mode of surface deformations is expected when $\mu_s \gg \mu_l h$. In this case, the relatively low viscosity of the interstitial fluid allows the surfactant monolayers to slide over one another (see figure 11(b)). Under this hypothesis, the surface tensions on each side of the outer soap films can be different, and are denoted γ_{int} and γ_{ext} respectively. As indicated before, over the whole range of sollicitations explored, the total surface area of each bubble is found to be constant so that the internal monolayer does not experience any significant compression or stretching. It yields that γ_{int} is constant equal to γ_0 . The contact angle deviation $\Delta\theta_d$ thus only results from the modulation of γ_{ext} associated with the compression and stretching of the external monolayer, so that:

$$\sqrt{3}\gamma_0\Delta\theta_d(t) = \Delta\gamma_{ext}(t) \quad (15)$$

Following the same scheme as before, the associated G' and G'' can be expressed as in equations (12) and (13), with a geometrical factor f now equal to:

$$f(r_c^0, R) = \frac{1}{\sqrt{3}} \frac{2r_c^{02}}{2R^2 - r_c^{02}} \quad (16)$$

Figure 12 shows the frequency diagram of E' and E'' together with $\gamma_0 G'/f$ and $\gamma_0 G''/f$ calculated from the same set of data as in figure 9, within both (a) the adhesive and (b) the sliding monolayers hypothesis. It appears that none of these models correctly captures the viscoelastic adhesive properties of the bubbles. The stored and dissipated energy in the oscillating double bubbles experiments are overestimated in the first model and underestimated by the second one.

Bulk and surface viscosities for the same solution (TTAB in a water/glycerol mixture) have been determined by Pitois et al. [27]. They found $\mu_l = 2.10^{-3} Pa.s$ and $\mu_s = 2.10^{-8} kg.s$. Estimating the film thickness to be of the order of a few μm , this yields a ratio $\frac{\mu_l h}{\mu_s}$ of the order of a few tenth, which is not incompatible with an intermediate regime of film deformation.

6 Application to a 2D model foam

In this part, the consequence of such dynamic effects on the bulk rheology of foams is discussed. We attempt to estimate how the angular measurements provided by the double bubble set-up can be relevant to predict the contribution of the films (and Plateau borders) to the foam rheological properties. Our approach will be limited to a perturbative version of Princen 2D regular hexagonal model. Figure 13(a) shows the initial configuration, where r is the initial (and uniform) length of the films. As a reference situation, we consider the quasistatic deformation of the structure associated with an imposed strain ϵ along the horizontal direction. Taking into account Plateau rule and

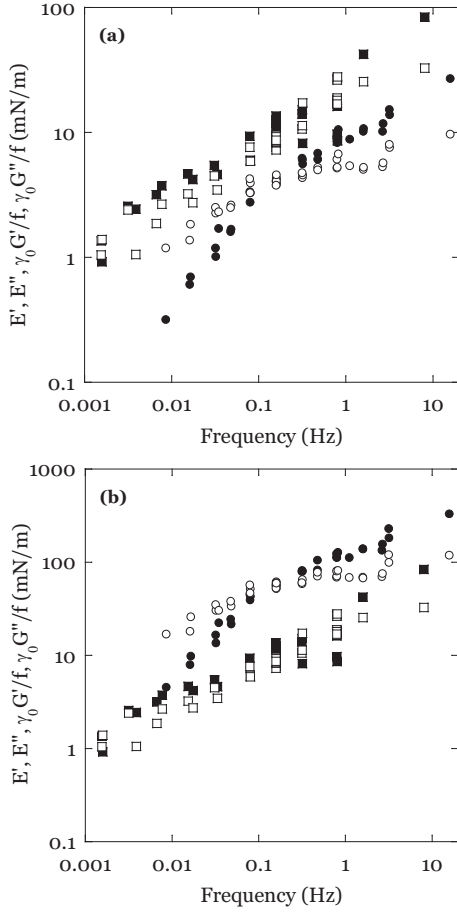


Figure 12. Comparison of the Gibbs moduli E' (closed squares) and E'' (open squares) obtained from the oscillating bubble experiments, with $\gamma_0 G'/f$ (closed circles) and $\gamma_0 G''/f$ (open circles). The later correspond to the angular moduli measured with the double bubble experiments and normalized by the geometrical parameter $f(r_c^0, R)$. (a) Model of adhesive monolayers: $f(r_c^0, R) = \frac{2}{\sqrt{3}} \frac{4R^2}{(2R^2 - r_c^{02})}$ (b) Model of sliding monolayers: $f(r_c^0, R) = \frac{1}{\sqrt{3}} \frac{2r_c^{02}}{2R^2 - r_c^{02}}$.

the surface conservation of each cell, Princen derives the angle Ψ of the initially vertical films as well as the film length variation dr as a function of ϵ (see figure 13(b)):

$$\Psi = \frac{1}{2}\epsilon \quad (17)$$

$$\frac{dr}{r} = \frac{\sqrt{3}}{2}\epsilon \quad (18)$$

The shear stress on a horizontal line (indicated in figure 13(b)) can be evaluated by considering that each film crossing this plane has a contribution $F = 2\gamma \sin(\Psi)$. Since the width of a unit cell is $r\sqrt{3}$, the stress is written:

$$\sigma = F = \frac{2\gamma}{r\sqrt{3}} \sin(\Psi) \approx \frac{2\gamma}{r\sqrt{3}} \Psi \quad (19)$$

This allows one to define a shear modulus:

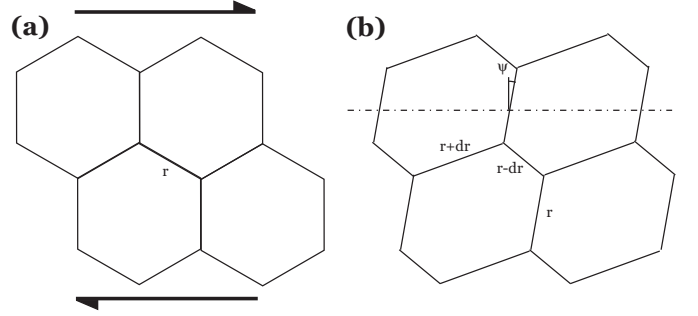


Figure 13. Princen model for the deformation of a 2D hexagonal foam. (a) Initial configuration. (b) After a small quasistatic deformation, the angles of the Plateau border remain equal to 120° . To the first order, the vertical films length remains unchanged but their orientation change by an angle ψ . The other films length are modified by a quantity dr proportional to the applied strain.

$$\mu = \frac{\sigma}{2\epsilon} = \frac{\sqrt{3}\gamma}{2r} \quad (20)$$

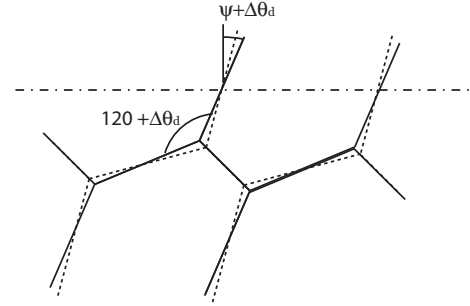


Figure 14. Effect of the dynamic contact angle correction on the deformation of a 2D hexagonal structure. Contrary to the classical quasistatic deformation (dashed line), the angle of the central Plateau border is no longer 120° . This deviation induces an additional rotation of the vertical line of an angle equal to the dynamic correction $\Delta\theta_d$.

The system is now submitted to an oscillating strain $\epsilon = \epsilon_0 \cos(\omega t)$. At finite oscillating frequency, one expects the Plateau rule to no longer be obeyed, and a correction $\Delta\theta_d(t)$ has to be added to the angle Ψ (see figure 14). By analogy with the double bubble measurements, we define G' and G'' such as:

$$\Delta\theta_d(t) = G'(\omega) \frac{dr}{r} \cos(\omega t) + G''(\omega) \frac{dr}{r} \sin(\omega t) \quad (21)$$

In the limit where the structure is weakly perturbed with regards to its equilibrium configuration (i.e. $\Delta\theta_d \ll \Psi$), the expression of dr/r provided by Princen (equation 18) remains valid to the first order. Substituting ψ by $\psi + \Delta\theta_d$ in equation 19 yields a corrected foam modulus which complex form now writes:

$$\tilde{G} = \mu[1 + \sqrt{3}(G' + iG'')] \quad (22)$$

It should be noticed that this result is independent of the physical origin of the viscoelastic process which sets G' and

G'' . With the solution used in the present study, it appears that the viscoelastic behavior of the films is responsible for the observed deviation to Plateau rule. But one might expect for other systems that the dominating effect is the viscous dissipation localized in the Plateau border. Regardless of this underlying mechanism, the frequency diagram provided by the double bubble angular measurement directly provides the contribution of the film and Plateau border rheology to the foam modulus.

One limitation of this approach however needs to be underlined. Princen model of foam elasticity is based on a perfectly regular network. In a real foam, r is largely distributed and one expects G' and G'' to depend on the relative lengths of the films connecting the given vertex. One is actually confronted with the same averaging problem when trying to evaluate the macroscopic modulus μ of a disordered film network. This structure parameter should control the prefactor of $G' + iG''$. But this limitation should still allow to compare different systems (with different film rheological properties) provided that the foam structure is identical (same polydispersity).

Conclusion

A device has been developed to measure the contact angle between two soap bubbles in static and dynamic adhesion. This set-up allows us to confirm the existence of a negative line tension associated with the presence of a Plateau border at the intersection of three soap films: the static contact angle is systematically larger than 120° and the deviation amplitude can be quantitatively predicted given the central film radius and volume of the Plateau border. By varying the distance between bubbles, one can modulate the radius r_c of the central film. This induces a further deviation of the contact angle $\Delta\theta_d$ which maximum value scales linearly with the amplitude of $\Delta r_c/r_c$. The amplitude and phase shift of $\Delta\theta_d$ with regards to $\Delta r_c/r_c$ has been systematically studied as a function of the modulation frequency.

The resulting phase diagram exhibits a transition from a viscous to an elastic regime with a crossover at a frequency of order 0.2Hz. This behavior of the double bubble cannot be deduced in a straightforward way from measurements of the film rheology obtained by single oscillating bubble measurements. In particular, considering the three films in the double bubble experiment as being independently stretched leads to overestimate the stored and dissipated energy in the oscillating experiment. This indicates that the sollicitation to which monolayers are submitted in a foam are not equivalent to what is imposed in standard film rheometers. We suggest that this discrepancy results from the fact that self-supported Plateau borders do not act like solid barriers and that they may allow partial transfer of surfactant from one side to another. The limiting case, which was examined also, corresponds to the situation in which surfactant layers are free to slide over one another.

In order to test this hypothesis, we intend to vary the relative viscosity of the surfactant monolayer and the bulk solution. Surface viscosity can be increased by adding dodecanol in the solution. In contrast, the interstitial film can be rendered more viscous by increasing glycerol concentration or by adding soluble polymers such as PEO (Polyethylene Oxide).

We have illustrated the possibility to use these angular measurements as a way to predict the contribution of the films and vertices to macroscopic foam rheology. The proposed approach is based on a perturbative version of Princen 2D regular foam model. It is therefore extremely naive and will need further work in order to be adapted to 3D foams and to take into account structural disorder. However, it suggests that this type of geometrical measurements might provide most of the relevant information. In particular, it integrates the different modes of energy dissipation, including the viscous drag associated with the Plateau borders motion. In order to test these ideas, such dynamical adhesion data need to be confronted to standard rheological measurements on 3D foams for various chemical solutions.

We would like to thank K.Brakke for his help with Surface Evolver simulations as well as I. Cantat and J.-F. Géminard for fruitful discussions.

References

1. S.A. Khan, C.A. Schnepper, R.C. Armstrong, *J. Rheol.* **32**(1), 69 (1988)
2. D. Weaire, S. Hutzler, *The Physics of Foams* (Oxford University Press, New York, 1999)
3. R. Höhler, S. Cohen-Addad, *Journal of Physics: Condensed Matter* **17**, R1041 (2005)
4. D. Buzza, C.Y. Lu, M. Cates, *Journal de Physique II* **5**(1), 37 (1995)
5. L. Schwartz, H. Princen, *Journal of Colloid and Interface Science* **118**(1), 201 (1987)
6. J. Lucassen, M. Van den Tempel, *Journal of Colloid and Interface Science* **41**(3), 491 (1972)
7. J. Lucassen, M. Van den Tempel, *Chemical Engineering Science* **27**(3), 1283 (1972)
8. V. Bergeron, *Journal of Physics: Condensed Matter* **11**, R215 (1999)
9. H. Fruhner, K.D. Wantke, *Colloids and Surfaces, A: Physicochemical and Engineering Aspects* **114**, 53 (1996)
10. K.D. Wantke, H. Fruhner, *Journal of Colloid and Interface Science* **237**(2), 185 (2001)
11. P. Aussillous, D. Quéré, *Europhysics Letters* **59**(3), 370 (2002)
12. I. Cantat, R. Delannay, *Physical Review E* **67**(3), 031501 (2003)
13. N. Denkov, V. Subramanian, D. Gurovich, A. Lips, *Colloids and Surfaces, A: Physicochemical and Engineering Aspects* **263**, 129 (2005)
14. E. Terriac, J. Etrillard, I. Cantat, *Europhysics Letters* **74**(5), 909 (2006)
15. M. Durand, H.A. Stone, *Physical Review Letters* **97**(22), 226101 (4) (2006)
16. H.M. Princen, *Journal of Colloid and Interface Science* **91**(1), 160 (1983)
17. J. Plateau, *Statique Expérimentale et Théorique des Liquides Soumis aux Seules Forces Moléculaires* (Clemm, Paris, 1873)
18. M. Fortes, M. Rosa, *Journal of Colloid and Interface Science* **241**(1), 205 (2001)
19. J. Rodriguez, B. Saramago, M. Fortes, *Journal of Colloid and Interface Science* **239**, 577 (2001)
20. J.C. Géminard, A. Zywockinski, F. Caillier, P. Oswald, *Philosophical Magazine Letters* **84**(3), 199 (2004)

21. M. Fortes, P. Teixeira, *Philosophical Magazine Letters* **85**(1), 21 (2005)
22. M. Fortes, P. Teixeira, *Physical Review E* **71**, 051404 (2005)
23. K. Brakke, *Experimental Mathematics* **1**, 141 (1992)
24. S. Cohen-Addad, R. Höhler, Y. Khidas, *Physical Review Letters* **93**(2), 028302 (2004)
25. J. Gibbs, *Collected Works*, Vol. 1 (Dover Publishing Co. Inc, New York, 1961)
26. D. Langevin, *Advances in Colloid and Interface Science* **88**, 209 (2000)
27. O. Pitois, C. Fritz, M. Vignes-Adler, *Colloids and Surfaces, A: Physicochemical and Engineering Aspects* **261**(1-3), 109 (2005)